



Electrothermally activated microchips for implantable drug delivery and biosensing

John M. Maloney, Scott A. Uhland, Benjamin F. Polito, Norman F. Sheppard Jr.,
Christina M. Pelta, John T. Santini Jr. *

MicroCHIPS, Inc., 6-B Preston Court, Bedford, MA 01730, United States

Received 1 March 2005; accepted 15 August 2005

Abstract

Novel drug delivery and biosensing devices have the potential to increase the efficacy of drug therapy by providing physicians and patients the ability to precisely control key therapy parameters. Such “intelligent” systems can enable control of dose amount and the time, rate, and location of drug delivery. We have developed and demonstrated the operation of an electrothermal mechanism to precisely control the delivery of drugs and exposure of biosensors. These microchip devices contain an array of individually sealed and actuated reservoirs, each capped by a thin metal membrane comprised of either gold or multiple layers of titanium and platinum. The passage of a threshold level of electric current through the membrane causes it to disintegrate, thereby exposing the protected contents (drugs or biosensors) of the reservoir to the surrounding environment. This paper describes the theory and experimental characterization of the electrothermal method and includes *in vitro* release results for a model compound. © 2005 Elsevier B.V. All rights reserved.

Keywords: Microchip; Drug delivery; Biosensor; Implant; Microfabrication

1. Introduction

Pulmonary, transdermal, intravenous or subcutaneous injection or infusion, and implantable systems have been developed for situations where oral drug delivery is not optimal or feasible [1]. Implantable drug delivery devices are particularly desirable where compliance with a prescribed drug regimen is critical. Such devices

allow a drug to be delivered at a specific rate without regular physician or patient intervention. Currently available drug delivery implants can be divided into two main categories, based on whether they deliver drug in a passive or active manner. Polymer depots are the most common passive drug delivery systems. They are designed to maintain a constant diffusion rate of drug out of the polymer, or they degrade in the body at a particular rate, thereby releasing drug at that rate. Representative commercial products that employ this method include Gliadel® Wafers for malignant brain tumors and Zoladex® implants for prostate cancer.

* Corresponding author. Tel.: +1 781 275 1445; fax: +1 781 275 1446.

E-mail address: jsantini@mchips.com (J.T. Santini).

Similarly, Viadur® implants achieve continuous release of leuprolide acetate for prostate cancer through the use of osmotic pressure-generating agents that push drug out of a titanium tube. The primary disadvantage of these systems is that they cannot be actively controlled. Once implanted, they continue to release drug until they are removed or their drug supply is exhausted. Mechanical pumps are the most common active delivery systems. They are able to deliver drug in a pulsatile manner, in addition to being able to achieve continuous administration. However, implanted pumps are large, and they are limited to delivering liquid drug formulations. Most proteins have limited stability when stored in liquid form at body temperature, creating a significant hurdle for the broad use of this technology.

Protein drugs are not the only medical innovation that suffers from poor stability when placed in the body. The fouling of biosensor electrode surfaces or semi-permeable membranes with cells and proteins and the degradation or deactivation of required enzymes or reagents have made it nearly impossible to achieve long-term stability of implanted biosensors [2]. Past attempts to solve these problems have met with limited success and usually include the expensive and technically difficult task of modifying the sensor chemistry or device materials.

A desirable drug delivery or biosensor implant would be small in size, have the ability to protect the drug or biosensor from the body until needed, allow continuous and pulsatile delivery of both liquid and solid drug formulations, and be controllable by the physician or patient. An array of individually sealed reservoirs that can be opened on command to expose their contents to the body meets these criteria. One or more drug formulations are sealed in the reservoirs, protecting them from the body until the reservoir is opened and the drug is released. Alternatively, biosensors are sealed in the reservoirs to protect them from the biofouling that normally occurs in the body. Sensing is initiated by opening a reservoir to expose the biosensor to the body. The process of sequentially exposing new sensors as old ones foul enables long-term implanted sensing using currently available, short-term sensors.

There has been much interest in recent years in the application of microfabrication technology to drug delivery and biosensing [3–5]. Here we report on the development of an electrothermal mechanism for selectively exposing the contents of reservoirs formed

in a microfabricated device. The structure of this device is similar to the first controlled release microchip demonstrated experimentally in the literature, which employed an electrochemical release mechanism [6,7]. Individual reservoirs in that device were opened *in vitro* and *in vivo* by applying an electric potential to a gold membrane covering each reservoir. An electrochemical reaction created soluble gold complexes and caused the membrane to dissolve. The electrothermal mechanism presented here also employs a metal membrane over each reservoir, but these membranes are removed instead by local resistive heating from an applied current. This method has the advantage of being independent of the chemistry of the environment surrounding the device and is many times faster than the electrochemical method. In this paper, we describe the fabrication and testing of microchip devices intended for the selective exposure of multiple reservoirs. Device operation is characterized for membranes fabricated from two different material systems, and the results of an *in vitro* drug release study using a radiolabeled compound are also presented.

2. Materials and methods

2.1. Microchip fabrication

Devices for this study were produced using standard microfabrication processes [8,9], and a representative section of one such reservoir-based microchip is shown in Fig. 1. The primary components include reservoirs containing drug formulations or biosensors, metal

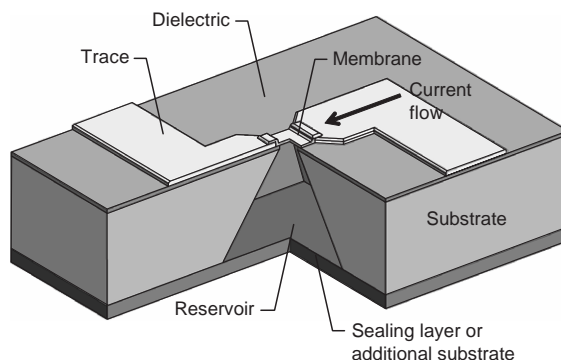


Fig. 1. A representative section of a reservoir-based microchip (ceramic passivation layer not shown).

membranes capping the reservoirs, and metal traces for directing electric current to the membranes. The fabrication process described herein incorporates two different metal layers, so that the membrane material and thickness can be decoupled from the trace material and thickness.

The starting material for the microchip fabrication process is a $\langle 100 \rangle$ -oriented, single crystal silicon wafer with a thickness of $525 \pm 2 \mu\text{m}$. A $0.2 \mu\text{m}$ layer of low-stress, silicon-rich silicon nitride is deposited on both sides of the wafer by low pressure chemical vapor deposition (LPCVD). This layer is used to electrically insulate metal features from the silicon substrate and serves as a support during the fabrication of the metal membranes.

Photolithography and reactive ion etching (RIE) are used to create openings in the silicon nitride on the back side of the wafer, and square pyramidal reservoirs are etched into the silicon using aqueous potassium hydroxide (25 wt.% KOH at 80°C). Etching initiates at the silicon areas exposed by RIE and continues through the wafer until suspended silicon nitride membranes are created on the front side of the wafer. The dimensions of the large and small openings of the pyramid-shaped reservoirs are 800×800 and $50 \times 50 \mu\text{m}^2$, respectively, which results in a reservoir volume of approximately 120 nL.

The traces are formed by sputter depositing a Au layer with a Ti adhesion layer and patterning the features by wet etching. The thickness of the traces varies across different chip configurations and is described below. The metal membranes are formed by combining sputter deposition with a liftoff process to create features that completely cover and overlap the edges of the suspended silicon nitride membranes. A ceramic passivation layer is deposited on the microchip by plasma enhanced chemical vapor deposition (PECVD) and is removed over the membrane area by photolithography and RIE. Finally, the silicon nitride membranes are removed from underneath the metal membranes by RIE.

The metal membranes for this study were composed of either Au or Pt/Ti/Pt. The Au and Ti base materials were chosen to represent relatively low- and high-resistivity metals, respectively. The Pt is added to protect the Ti with a noble, inert metal in vivo and during fabrication, when several RIE etching steps terminate on the membrane material. The silicon nitride

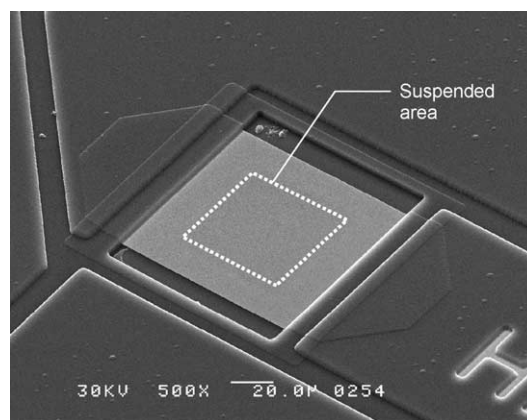


Fig. 2. Scanning electron micrograph of a microfabricated Au membrane over a $50 \times 50 \mu\text{m}^2$ reservoir opening (the dotted line was added to delineate the membrane area suspended over the reservoir).

support and ceramic passivation layers are etched by RIE with a CF_4/O_2 plasma, which also attacks Ti. The Pt layer provides an etch stop material that protects the membrane during these steps. A 10 nm Ti adhesion layer was used for both membrane compositions. This layer is also etched when the silicon nitride support layer is removed. A suspended Au membrane over a $50 \times 50 \mu\text{m}^2$ silicon opening is shown in Fig. 2.

Membrane activation was characterized on 100-reservoir microchips with traces composed of 10 nm Ti/2 μm Au/10 nm Ti. The membrane material was 300 nm Au or 20 nm Pt/300 nm Ti/20 nm Pt. There was an additional metal layer (10 nm Ti/300 nm Au/10 nm Ti) in the 100-reservoir Pt/Ti/Pt devices that served to electrically connect the traces with the Pt/Ti/Pt membrane. The ceramic passivation layer was 1 μm silicon oxide/1 μm silicon nitride/1 μm silicon oxide. The in vitro release study was performed on a 24-reservoir microchip with traces composed of 10 nm Ti/600 nm Au/10 nm Ti. The membrane material was 40 nm Pt/300 nm Ti/40 nm Pt. No passivation layer was used on this microchip. Microchips containing 24 and 100 reservoirs are shown in Fig. 3. Membrane composition is the most important factor in device operation, so differences in trace composition do not significantly affect membrane activation.

2.2. Electrothermal membrane activation

All metal membranes were inspected for defects using a light microscope and back side illumination.

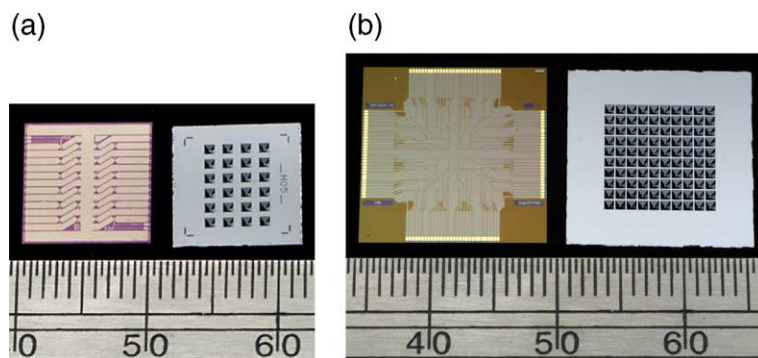


Fig. 3. Photographs of (a) 24-reservoir and (b) 100-reservoir microchips showing the front side (left) containing metal membranes and traces and the back side (right) containing reservoirs. A ruler with 1 mm increments is included for scale. [Photo credit: Dana Lipp Imaging].

Wire bonds were used to electrically connect the microchip to a printed circuit board, which was connected to the activation instrumentation by a ribbon cable. Membranes were electrothermally activated by using a custom automated tester that charged a capacitor to a programmed voltage and discharged it through the circuit, as shown schematically in Fig. 4. The automated system can turn off the current flow after a specified time or immediately after activation is completed, as detected by a decrease in current. The tester was programmed to apply a fixed pulse width of at least 100 μs in this study, and the current was measured at a sampling rate of 1 MHz (once per microsecond) by using a 0.1 Ω sense resistor in series with the activation circuit. The capacitor value was at least 470 μF in all studies, resulting in a time constant of voltage decay of at least 1 ms, which is far larger than the membrane activation time of 5–100 μs . Consequently, the voltage drop during activation was negligible.

Membranes on 100-reservoir chips were placed in a petri dish and activated in deionized (DI) water. The area of the opening in the metal membrane after

activation was measured by photographing the openings with back side illumination and analyzing the photographs with image processing software. The number of bright pixels counted in an activated membrane was then normalized to the number of pixels included in a fully open reservoir to determine the percentage of the membrane area opened under various activation conditions.

2.3. In vitro release

^{14}C -labeled mannitol was selected as the model compound for the in vitro release studies due to its ease of detection and quantification by liquid scintillation counting. The formulation used in this study was composed of 1% v/v sodium fluorescein solution (Sigma; #F-7137), 2% v/v PEG 200 (Union Carbide; Carbowax™ Polyethylene Glycol), and 97% v/v ^{14}C -labeled aqueous mannitol solution (PerkinElmer Life Sciences; #NEC13; specific activity 53.7 mCi/mmol; 1.0 mCi/ml).

Each reservoir of 24-reservoir microchips was filled with 100 nL of the mannitol formulation,

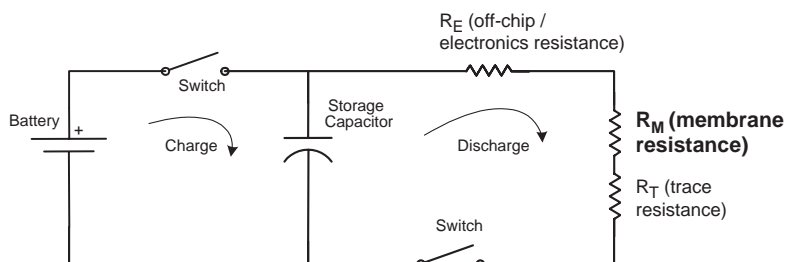


Fig. 4. Simplified schematic of a membrane activation circuit.

dispensed at a rate of 50 nL/s using a custom, automated filling station with a micro-syringe pump (World Precision Instruments; Ultra Micro Pump II and MICRO4 pump controller). The formulation was dried in a desiccator for 1 h. A silicon wafer containing KOH-etched reservoirs was used as a mold to make 50 nL square pyramid-shaped paraffin (Reed Wax #89041; $T_m=52\text{ }^\circ\text{C}$) inserts. One paraffin insert was placed in each of the filled reservoirs. The microchip was placed on a hot stage at $70\text{ }^\circ\text{C}$ to reflow the paraffin over the dried mannitol formulation. The microchip was then assembled in a custom flow cell and sealed by compressing elastomeric gaskets against the front and back sides of the microchip as shown in Fig. 5. Assembly of the flow cell created a chamber that was filled with phosphate-buffered saline (PBS). Periodically, the fluid was replaced via inlet and outlet tubes and the collected fractions were analyzed. An automated system was used to activate membranes, control the flow of fluid through a test chamber, and recover the contents following each release event. The flow cell containing the microchip was placed on a microscope stage to observe and video record releases.

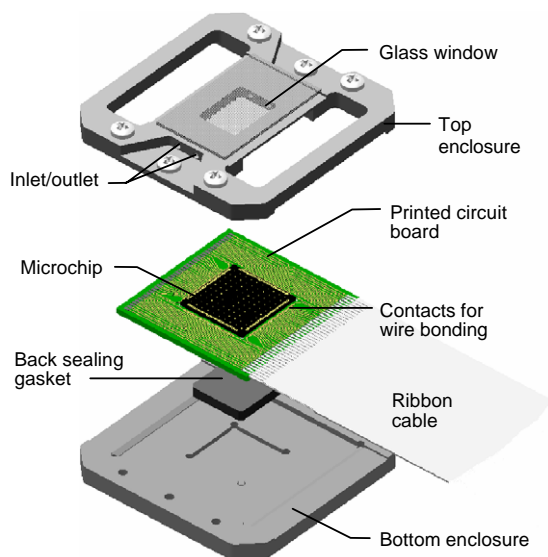


Fig. 5. Schematic of a typical flow cell for in vitro release studies (front side gasket not shown).

Release of drug from individual reservoirs was performed every 4 h. The fluid contained within the flow cell chamber was recovered on an hourly basis, resulting in four samples per release event. Three of the 24 reservoirs were not released during the in vitro study. The membranes of two reservoirs were occluded by the front side gasket, and a third reservoir was not released due to known variability in the amount of material in the first reservoir filled. The quantity of ^{14}C -labeled mannitol in each fraction was determined by liquid scintillation counting (Packard 1900 TR). Control samples were prepared by filling several unsealed reservoirs on a microchip, immersing the chip in PBS, and assaying the contents for radioactivity. The radioactivity in each reservoir of the control sample averaged 182 nCi.

3. Results and discussion

3.1. Electrothermal activation mechanism

The membrane activation process is similar to the operation of an electrical fuse. Current is passed through the traces and membrane to rapidly heat the membrane to the point of failure to expose the contents of a particular reservoir. Heating occurs preferentially in the membrane for several reasons. First, the membrane is suspended in an environment with a lower thermal conductivity than the silicon substrate. Second, the membrane has a smaller cross-sectional area than the traces, resulting in increased current density and resistive heating. Third, the membrane may be made from a material that is more resistive than the trace material, increasing heat generation.

Membrane failure occurs as quickly as $5\text{ }\mu\text{s}$ after the application of the activation current, briefly exposing tissue, drug, or biosensor components to elevated temperatures. The magnitude of the instantaneous current depends upon the applied voltage and the membrane material and dimensions and ranges from 0.3–5.6 A for the devices used in this work.

There is no longer a barrier between the contents of the reservoir and the external environment after the membrane is removed. Stored drugs are released by dissolution and diffusion through the newly created opening or, alternatively, molecules in physiological

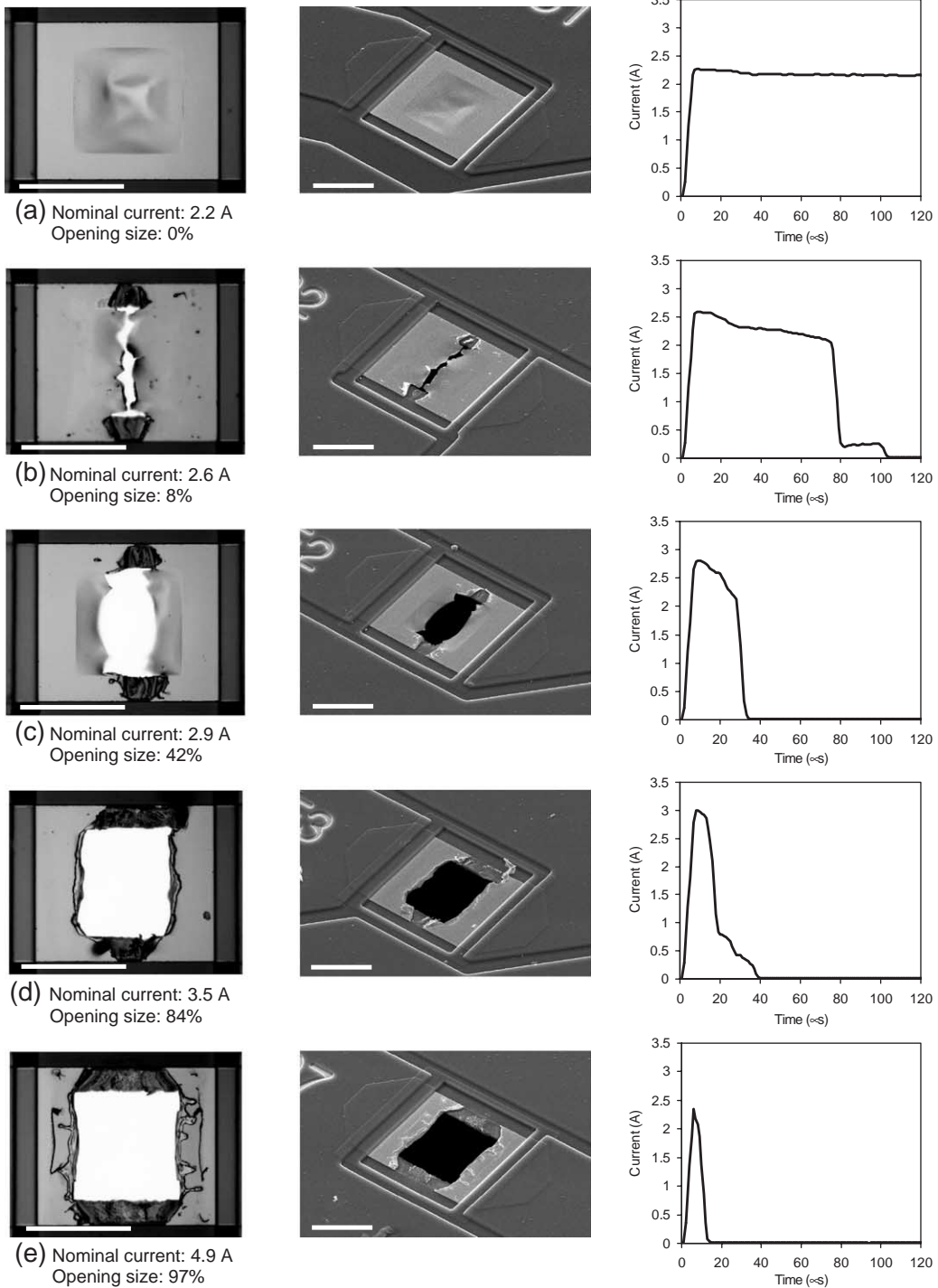


Fig. 6. Light micrographs (left), scanning electron micrographs (middle), and activation currents (right) for five Au membranes (suspended area $50 \times 50 \mu\text{m}^2$) activated in water. The scale bar represents $50 \mu\text{m}$ in all images.

fluid can diffuse into the reservoir to contact a stored biosensor. Successful reservoir activation is confirmed by observing an increase in total circuit resistance caused by the partial or complete removal of the membrane current path.

A disadvantage of using the same material and cross-sectional area for both the membranes and the traces is a relatively low power efficiency, since the traces are much longer than the membrane. In this hypothetical case, most of the input power during activation dissipates in the traces and does not contribute to the electrothermal membrane removal process. Decoupling the membrane and trace fabrication processes provides the opportunity to incorporate different materials and vary cross-sectional areas to improve power efficiency. This is especially important for implantable electronic devices, where device size is a critical parameter. High power efficiency can reduce implant size by allowing the use of a smaller battery and electronic components.

The power dissipated in the membrane represented in the circuit diagram of Fig. 4 is

$$P_M = I^2 R_M = \frac{V^2 R_M}{(R_M + R_T + R_E)^2} \quad (1)$$

where I is the current, V is the capacitor charging voltage, R_M is the membrane resistance, R_T is the trace resistance, and R_E is the electronics (off-chip) resistance. The amount of heat generated in the membrane can be increased by decreasing the resistance of the traces, thereby increasing the current flow at a given voltage. Membrane heat generation can also be increased by increasing the membrane resistance. The power efficiency is maximized when the membrane resistance equals the sum of the other resistances in the circuit (this is the principle of matching source and load resistances).

$$R_M = R_T + R_E \quad (2)$$

R_T and R_E were each approximately 1Ω for the devices and activation circuit used in this study, and R_M was 0.15Ω for Au membranes and 1.5Ω for Pt/Ti/Pt membranes.

Membrane activation is characterized by comparing an input parameter with an operational result. Activation current is used as the controllable input parameter because resistive heat generation is a

function of the current density. The membrane opening area following activation is a critical operational parameter, since drug release or sensor exposure over time is controlled largely by mass transport through the opening. We have therefore characterized the activation of Au and Pt/Ti/Pt membranes by passing a range of currents through different membranes and measuring the resulting opening area. The use of current instead of voltage allows us to decouple the results of our membrane characterization experiments from test platforms with different circuit resistances.

The physical medium in contact with the membrane surfaces can have a significant impact on device performance due to heat conduction to the microchip surroundings. For example, a membrane activated in water (thermal conductivity $k=0.6 \text{ W/m K}$) requires more current than a membrane activated in air ($k=0.026 \text{ W/m K}$) because more of the heat generated in the air case is retained by the membrane. Water was used on both sides of the membranes in our activation experiments to simulate in vivo operating conditions. Each chip was inspected before testing to ensure that no air bubbles were in contact with the membrane surface.

Results from the activation of Au and Pt/Ti/Pt membranes are shown in Figs. 6–9. Light micrographs, scanning electron micrographs, and activation currents for selected Au membranes are shown in Fig. 6. The current increases initially as the voltage is applied to the traces. The current then decreases for two reasons related to the membrane resistance. The first is the

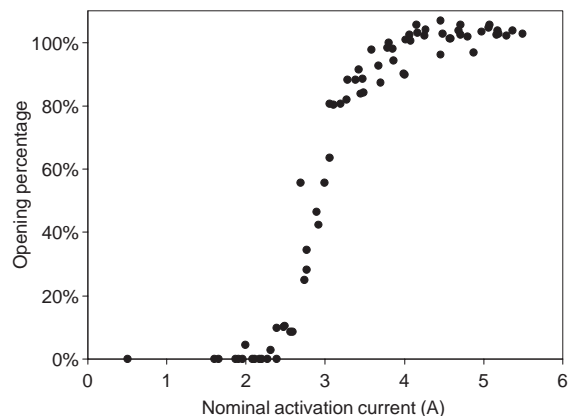


Fig. 7. Membrane opening area vs. activation current for Au membrane activation in water.

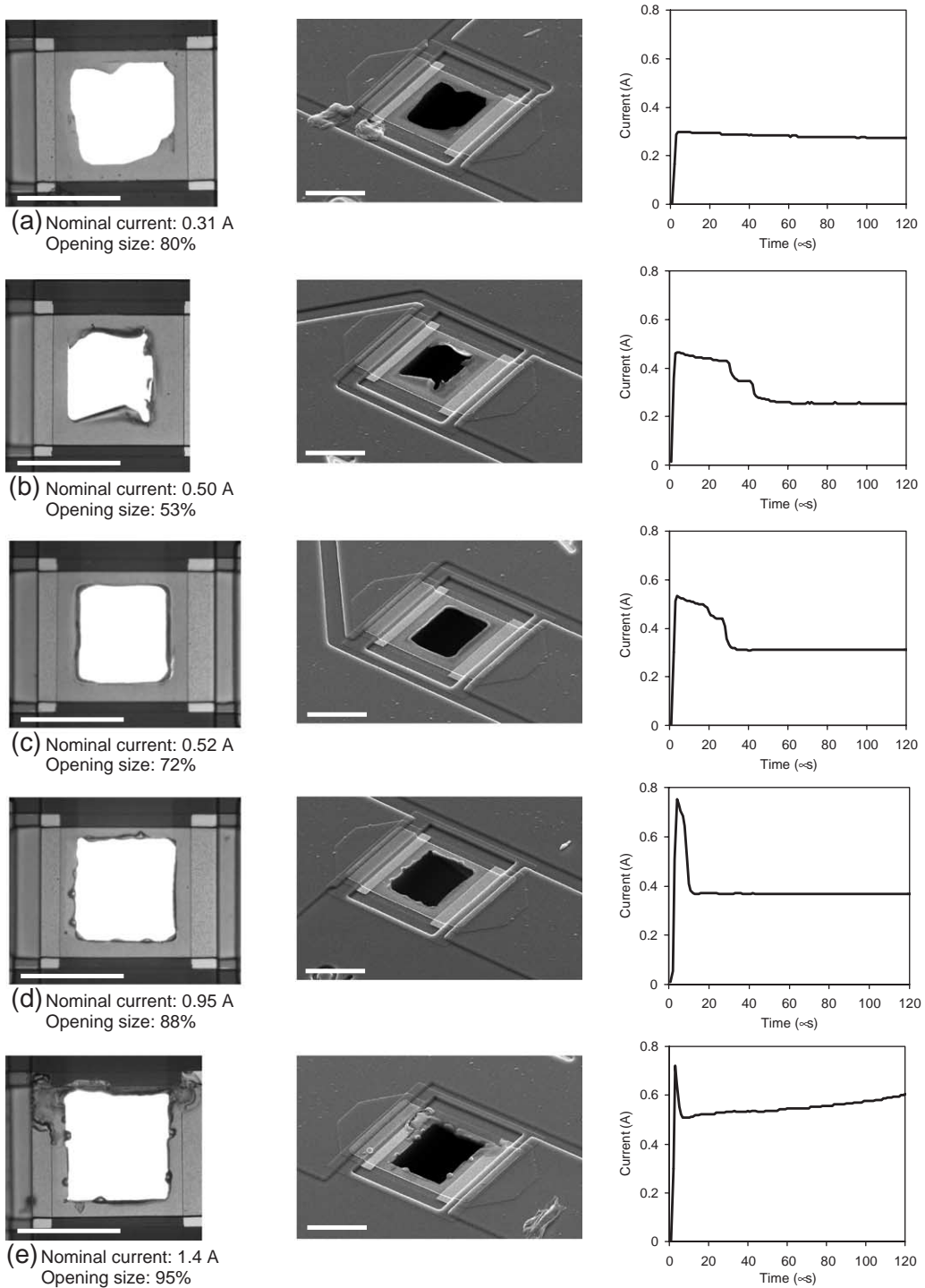


Fig. 8. Light micrographs (left), scanning electron micrographs (middle), and activation currents (right) for five Pt/Ti/Pt membranes (suspended area $50 \times 50 \mu\text{m}^2$) activated in water. Scale bar represents $50 \mu\text{m}$ in all images.

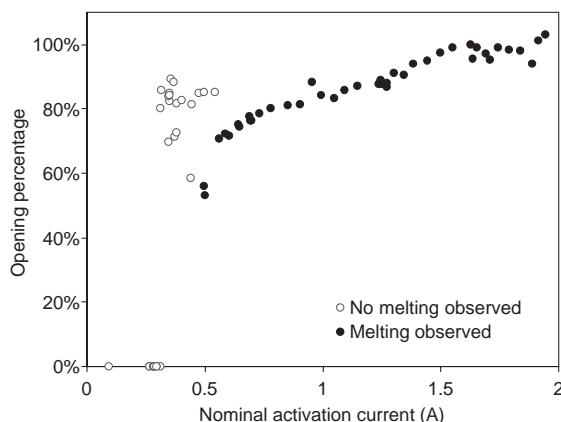


Fig. 9. Membrane opening area vs. activation current for Pt/Ti/Pt membrane activation in water.

positive temperature coefficient of resistivity of Au as the membrane temperature increases. The second is the reduction in cross-sectional area for current flow as the membrane fails. The membrane opening area increases with current as the activation process becomes more energetic.

A nominal current value is quoted for each activation event because the instantaneous current varies with time. The nominal value is calculated by dividing the applied voltage by the circuit resistance measured before activation. Since membrane resistance increases during activation, the nominal current represents the maximum possible current through the circuit. When the activation current is relatively low, as in Fig. 6(a), (b), and (c), the observed peak current is approximately equal to this nominal current. As the activation current is increased, the membrane begins to fail within microseconds, and the resolution of current detection is limited by the 1 MHz sampling rate.

The membrane opening area as a function of activation current for seventy-five Au membranes is plotted in Fig. 7. These membranes were fabricated on a single 100-reservoir chip. This chart includes the data points shown in Fig. 6.

Light micrographs, scanning electron micrographs, and activation currents for selected Pt/Ti/Pt membranes are shown in Fig. 8. There are several important differences between Au and Pt/Ti/Pt membrane activation. First, less current is required to rupture the Pt/Ti/Pt membranes than the Au membranes. The primary reason that the Pt/Ti/Pt membranes open more effi-

ciently may be attributed to the much greater resistivity of Pt/Ti/Pt relative to Au. Consequently, the resistive heat generation is much larger for a given current. The resistance of the Pt/Ti/Pt membranes approximates the sum of the resistances of the traces and the off-chip electronics in the 100-reservoir chip configuration, so the operating point approaches the optimum power-matching balance.

Second, the membrane sides, or the portions of the Pt/Ti/Pt membrane in contact with the silicon, remain after activation for nominal currents less than 1.4 A. This difference may be attributed to differences in the material properties of Au and Pt/Ti/Pt membranes. The larger thermal conductivity of Au allows more heat to pass from the center of the membrane to the edges on the silicon, which can cause the sides to increase in temperature and melt. Additionally, the smaller resistivity of Au results in a smaller perturbation in current as the membrane fails. The Au membrane represents only a small fraction of the total circuit resistance, so the reduction in cross-sectional area during failure has relatively little impact on the current until the sides have almost completely failed. In contrast, the Pt/Ti/Pt membrane represents approximately half of the total circuit resistance. The reduction in cross-sectional area once the suspended portion of the membrane has failed has a significant effect on current, which is reduced below the level capable of melting the sides.

Third, an operating regime was observed for Pt/Ti/Pt membranes in which rupture occurred without any signs of melting. This effect, which occurred at nominal currents of approximately 0.3–0.5 A, produced variable opening sizes. At larger currents, the opening size increased monotonically with applied current and signs of melting were observed, as they were with Au membranes. Additionally, the “no melting observed” effect was seen only when membranes were activated in liquid. The formation of vapor bubbles when the device is immersed in liquid may rupture the membrane by a fracture mechanism before the membrane temperature increases to the melting point of Ti or Pt.

Fig. 9 is a plot of the membrane opening size as a function of activation current for fifty Pt/Ti/Pt membranes fabricated on a single 100-reservoir device. This chart includes the data points shown in Fig. 8. A preferred range of activation currents exists where the opening size and activation time do not change greatly

with small changes in current. In general, Pt/Ti/Pt membranes are favored over Au membranes because the required activation current is lower.

3.2. In vitro release

A microchip with Pt/Ti/Pt membranes was used for the in vitro release study, and the membranes were activated at sufficient current to lie in the “melting observed” region shown in Fig. 9. Every addressed reservoir successfully opened and released its contents during the in vitro release study, as confirmed by resistance measurements, analysis of the electrical activation signals, and direct visual assessment. The cumulative amounts of ¹⁴C-labelled mannitol recovered per release for each of twenty-one releases and per release after 4 h are shown in Figs. 10 and 11, respectively. The average amount recovered from each reservoir during the 4 h following membrane activation was 179 nCi, or 99% of the average control amount. The standard deviation among the twenty-one releases was 8 nCi, and the coefficient of variation was 4%. This study demonstrates that activation using the electrothermal mechanism is reliable and repeatable.

3.3. Electrothermal analysis

Refrozen membrane metal around the edge of the reservoir opening was observed, indicating that the melting temperature of Au (1064 °C), Ti (1670 °C), or Pt (1770 °C) is exceeded during membrane activation.

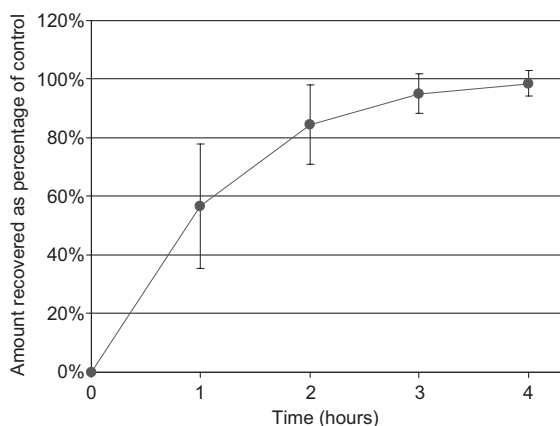


Fig. 10. In vitro release results: cumulative amount of ¹⁴C-mannitol recovered from each of twenty-one reservoirs over a 4-h period.

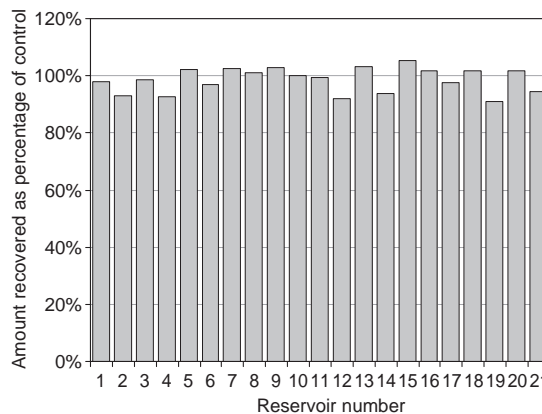


Fig. 11. In vitro release results: total amount of ¹⁴C-mannitol recovered over a 4-h period from each reservoir.

Vapor bubbles form on the membrane surface, as observed with high-speed photography. The vapor barrier serves to thermally insulate the membrane because the thermal conductivity of water vapor is significantly less than the thermal conductivity of liquid water. The short duration of energy input into the membrane and the presence of an insulating vapor layer on the membrane surface allows more of the energy dissipated in the membrane to melt the membrane.

The potential for thermal exposure to tissue or to a stored drug or biosensor during Pt/Ti/Pt membrane activation was assessed by calculating the energy dissipated and the temperature rise. Much less heat generation occurs around the traces than around the membranes because the resistivity of the Au traces is far lower than the Pt/Ti/Pt membranes. Consequently, the energy dissipated at the membrane was evaluated rather than at the traces. The activation time is assumed to be 10 μs, which corresponds to a nominal current of approximately 1 A and an opening area of over 80% for a 50 × 50 μm² membrane.

The energy dissipated in the area of the membrane during activation, E_M , can be calculated by

$$\begin{aligned}
 E_M &= \int P_M dt = \int I^2 R_M dt \\
 &= \int [VI - I^2(R_T + R_E)] dt
 \end{aligned}
 \tag{3}$$

The membrane resistance, R_M , varies with time and is not explicitly measured. Therefore, the integrand is

rewritten in terms of the voltage and trace and electronic resistances, which do not change during activation, and current, which is measured over time. A 10 μ s activation time yields an energy dissipation, E_M , of approximately 25 μ J for a $50 \times 50 \mu\text{m}^2$ Pt/Ti/Pt membrane.

The amount of material that could be heated with the energy dissipated during membrane activation relates to potential thermal exposure to tissue, drug formulations, or sensor reagents. The maximum temperature rise in a known volume of liquid results when all energy dissipated by the membrane is applied toward increasing the liquid temperature. The assumption that temperature-sensitive materials (cells, proteins, drug molecules, sensor reagents) will always reside in a liquid or solid environment, whether or not a vapor bubble at the membrane surface is present, allows determination of the potential thermal exposure to tissue or reservoir contents. For example, designating 10 °C as an undesirable temperature increase and modeling interstitial fluid and a drug formulation with the properties of liquid water, it is found that 25 μ J of energy can expose a maximum volume of 0.6 nL to this temperature. This volume is only approximately 0.5% of the reservoir volume of 120 nL. This estimate is conservative. The exposed volume is expected to be smaller because portions of the energy dissipated are distributed to both sides of the membrane, and some of this energy is dissipated directly into the silicon substrate. There is evidence that proteins can withstand even higher temperatures when the exposure time is extremely small. For example, one study showed that even at temperatures near 100 °C, it can take up to 300 μ s to denature the protein chymotrypsin [10]. Therefore, the likelihood of deleterious thermal exposure to tissue or reservoir contents during membrane activation is low due to short activation times and small affected volumes.

4. Conclusions

We have developed a microfabricated device that exposes sealed reservoirs controllably and independently. The device uses an electrothermal mechanism for rupturing a membrane to release drugs or expose biosensors. This mechanism was characterized by applying a range of currents to membranes composed

of two different material systems and evaluating the area and appearance of the resulting openings. An in vitro release test of a model compound demonstrated that the exposure mechanism is robust and reproducible. Finally, an analysis was performed with the membrane activation data to estimate the potential thermal exposure to tissue or stored drugs or sensor reagents.

This microfabricated device can be the core component of a fully implantable, intelligent system for the controlled release of potent therapeutic compounds that might otherwise require frequent injections or complex dosing regimens, including pulsatile release, continuous release, or the release of multiple drugs. Such a system can also protect biosensors that are prone to failure due to biofouling and expose them to the body when needed. Integration of wireless communication technology would allow non-invasive therapy modification by physicians, and possibly patients, with a choice of pre-programmed operation or release/exposure-on-command. By combining the capabilities for drug delivery and sensing, a closed-loop system can be developed in which therapeutic drugs are released automatically in response to a biosensor signal.

Acknowledgments

We would like to thank Je Kong for designing the membrane activation circuit, Dr. Zouhair Sbiaa and Dr. Michael Finot (Micalyne, Inc., Edmonton, Canada) for producing the microchips used in this study, and all other members of the MicroCHIPS team for their support of this work.

References

- [1] R. Langer, Where a pill won't reach, *Sci. Am.* 288 (4) (2003) 50–57.
- [2] N. Wisniewski, F. Moussy, W.M. Reichert, Characterization of implantable biosensor membrane fouling, *Fresenius' J. Anal. Chem.* 366 (2000) 611–621.
- [3] S.L. Tao, T.A. Desai, Microfabricated drug delivery systems: from particles to pores, *Adv. Drug Deliv. Rev.* 55 (3) (2003) 315–328.
- [4] A.C. Richards Grayson, R.S. Shawgo, A.M. Johnson, N.T. Flynn, Y. Li, M.J. Cima, R. Langer, A BioMEMS review:

- MEMS technology for physiologically integrated devices, Proc. I.E.E.E. 92 (1) (2004) 6–21.
- [5] A.C. Richards, I.S. Choi, B.M. Tyler, P.P. Wang, H. Brem, M.J. Cima, R. Langer, Multi-pulse drug delivery from a resorbable polymeric microchip device, Nat. Mater. 2 (2003) 767–772.
- [6] J.T. Santini, M.J. Cima, R. Langer, A controlled-release microchip, Nature 397 (1999) 335–338.
- [7] Y. Li, R.S. Shawgo, B. Tyler, P.T. Henderson, J.S. Vogel, A. Rosenberg, P.B. Storm, R. Langer, H. Brem, M.J. Cima, In vivo release from a drug delivery MEMS device, J. Control. Release 100 (2) (2004) 211–219.
- [8] M.J. Madou, Fundamentals of Microfabrication, 2nd ed., CRC Press, Boca Raton, FL, 2002.
- [9] S. Wolf, R.N. Tauber, Silicon Processing for the VLSI Era, 2nd ed. Process Technology, vol. 1, Lattice Press, Sunset Beach, CA, 2000.
- [10] G. Hüttmann, R. Birngruber, On the possibility of high-precision photothermal microeffects and the measurement of fast thermal denaturation of proteins, IEEE J. Sel. Top. Quantum Electron. 5 (4) (1999) 954–962.